Journal of Molecular Spectroscopy 375 (2021) 111395

Contents lists available at ScienceDirect

Journal of Molecular Spectroscopy

journal homepage: www.elsevier.com/locate/jms

Experimental observation of the $\nu_2+4\nu_3$ bands of $HD^{16}O$ and $HD^{18}O$ between 14975 and 15275 cm^{-1}

S. Chandran [a], S. Dixneuf [a,1], J. Orphal [b,2], A.A. Ruth [a,*]

[a] Physics Department & Environmental Research Institute, University College Cork, Cork, Ireland
[b] Institute of Meteorology and Climate Research (IMK) – Atmospheric Trace Gases and Remote Sensing (ASF), Karlsruhe Institute of Technology (KIT), Hermann-von-Helmholtz-Platz 1, D-76344 Eggenstein-Leopoldshafen, Germany

ARTICLE INFO

Article history:
Received 16 September 2020
In revised form 17 November 2020
Accepted 21 November 2020
Available online 25 November 2020

Keywords:
Water isotopologues
Overtone combination bands
Near infra-red
$HD^{18}O$
$HD^{16}O$
Fourier transform-incoherent broadband cavity enhanced absorption spectroscopy (FT-IBBCEAS)
Trace gas sensing.

ABSTRACT

The $\nu_2+4\nu_3$ combination bands of $HD^{16}O$ and $HD^{18}O$ were measured using Fourier transform-incoherent broadband cavity-enhanced absorption spectroscopy (FT-IBBCEAS) with a spectral resolution of 0.08 cm^{-1}. The ro-vibrational lines of these bands were assigned through comparison with *ab-initio* molecular lines from the Tomsk variational calculation database (http://spectra.iao.ru/). For $HD^{18}O$ and $HD^{16}O$ in total 114 and 141 strong lines were assigned in the region between 14975.3 cm^{-1} and 15243.3 cm^{-1} and between 14998.5 cm^{-1} and 15274.7 cm^{-1}, respectively. While the very satisfactory agreement of line intensities was used for line assignments, a systematic average discrepancy of ~0.305 cm^{-1} in line positions was identified between the measured lines of $HD^{18}O$ and the theoretically predicted lines from the Tomsk database. Similarly for $HD^{16}O$, an approximate wavenumber difference of ~0.361 cm^{-1} was observed. The wavenumber accuracy of the Fourier transform cavity enhanced absorption spectrometer was confirmed on basis of concurrently measured $H_2^{16}O$ spectra in the region between 15254.2 cm^{-1} and 15376.9 cm^{-1} and corroborated the systematic shifts of the *ab initio* data. A few lines of the $\nu_1+4\nu_2+2\nu_3$ bands of $HD^{16}O$ and $HD^{18}O$ were also identified. The data are compared and discussed on basis of existing literature data.

1. Introduction

One reason for water vapor being the most important greenhouse gas in the Earth's atmosphere is its ubiquity. Hence, not only the most dominant isotopologue, $H_2^{16}O$ (relative abundance 0.997317), is of high relevance for atmospheric sciences, but also its deuterated isotopologues, such as $HD^{16}O$ or $HD^{18}O$ (relative abundances 3.10693×10^{-4} and 6.23003×10^{-7}, respectively) [1]. In the analysis of trace gas measurements, be it from *in situ* spectrometers or remote sensing instruments, the occurrence of absorption features of water isotopologues, affecting the retrieval of number densities of target species, is very common in many spectral regions. Thus, the knowledge of weak water absorption lines including isotopologues is important to enable the unambiguous identification of other trace species. The high relevance of the isotopic composition of water vapour for climatic and hydrological studies has been illustrated recently in the publication of a global database on stable water vapor isotope ratios ($\delta^{18}O$ and δD) with high temporal resolution [2]. Furthermore, new experimental data on water isotopologues, in conjunction with *ab initio* calculations [3,4] enable the improvement of the ground state potential energy surface (as well as wavefunctions for intensity calculations) of water and hence a more accurate prediction of rotation-vibration line positions for spectral regions where experimental data are either sparse or unreliable, or do not exist.

Singly deuterated water, HDO, has been the subject of many previous theoretical studies (see e.g. Refs. [1,5–9]). $HD^{16}O$ has been widely experimentally addressed at lower energies (<14115 cm^{-1}) [10–26], but above 14115 cm^{-1} a more limited number of experimental investigation exists to our knowledge [26–31].

$HD^{18}O$ in comparison has been much less focused on [32–34], not least because of its lower natural abundance, and experimental data in the visible region do not seem to be available in the literature.

Here we report experimental observations of the $\nu_2+4\nu_3$ bands of the deuterated water isotopologues $HD^{16}O$ and $HD^{18}O$ and their (partial) rotational assignments. The spectra were measured in the

* Corresponding author.
E-mail address: a.ruth@ucc.ie (A.A. Ruth).
[1] Present address: Bioaster Technology Research Institute – Bioassays, Microsystems & Optics Engineering Unit, 40 Avenue Tony Garnier, 69007 Lyon, France.
[2] Present address: Division 4 "Natural and Built Environment", Karlsruhe Institute of Technology (KIT), Kaiserstrasse 12, 76131 Karlsruhe, Germany.

https://doi.org/10.1016/j.jms.2020.111395
0022-2852/© 2020 The Authors. Published by Elsevier Inc.

spectral range from 14975 to 15275 cm^{-1} using Fourier transform-incoherent broadband cavity-enhanced absorption spectroscopy (FT-IBBCEAS). The spectral analysis focused on the line positions' accuracy in the measured spectra and on assignments based on the line intensities and positions from the Tomsk *abinitio* variational calculation database (http://spectra.iao.ru/) [35] (this database will be referred to as "*Tomsk database*" from here on). The accuracy of absolute line intensities was not investigated in this study. The spectral resolution was moderately high (~0.08 cm^{-1}), hence strong lines in the spectral region of the ν_2+4ν_3 band are sufficiently isolated and well separated from the corresponding band of the most abundant water isotopologue ($H_2^{16}O$) to enable unambiguous assignments. A few lines in the spectral region of concern were assigned to the ν_1+4ν_2+2ν_3 combination bands of singly deuterated water. Our findings for $HD^{16}O$ are compared with available literature data [9,27,28,35] and give confidence for the assignment of the new lines in $HD^{18}O$.

The new data presented here will be useful for new theoretical modelling of the ground state potential energy surface of the water molecule. Moreover, the data will be also helpful for the interpretation of observation and retrieval of data from satellite based remote sensing applications such as the Global Ozone Monitoring Experiment 2 (GOME-2) onboard the MetOp satellites [36] or the TROPOspheric Monitoring Instrument (TROPOMI) onboard the Copernicus Sentinel-5 precursor probe [37,38].

After outlining some experimental details in the next section, we will present the main results and assignments in Section 3, and discuss the data on basis of a comparison with database and literature data in Section 4, before the work reported here is concluded.

2. Experiment

2.1. Measurement method, components and parameters

The near IR spectra of the deuterated water isotopologues $HD^{16}O$ and $HD^{18}O$ were measured using Fourier transform-incoherent broadband cavity-enhanced absorption spectroscopy (FT-IBBCEAS) [39–41]. The general experimental setup has been reported previously [42–45] and specifics of the measurement arrangement are only briefly outlined here. The light source was a 6 W supercontinuum source (Fianium SC450-6) operating at a repetition rate of 50 MHz delivering pulses of ~5 ps duration. The broadband radiation (~500–1800 nm) was passed through a long-pass filter with a cut-on wavelength at 642 nm (15600 cm^{-1}). The light was spatially filtered and collimated before entering the optical cavity of length d ~ 644 cm. The optical cavity was formed by two di-electric plano-concave mirrors (Layertec GmbH, Germany) with a high reflectivity between 14200 and 15600 cm^{-1}. The experiment was carried out with a static cell; no mirror purge was applied. An IR optimized achromatic doublet was used for coupling the light exiting the cavity into a multimode fiber (~0.8 nm), which was connected to the entrance port (aperture size 0.5 mm) of a Fourier transform spectrometer (FTS; Bruker Vertex 80). On basis of a low pressure CO_2 spectrum the instrumental line shape was determined, and a spectral resolution of ~0.08 cm^{-1} was established employing Norton-Beer weak apodization (see also next section). The integration time used for measuring the spectrum was 120 min. For this acquisition time a signal-to-noise ratio of >35 was achieved, which was evaluated on basis of the strong $HD^{16}O$ absorption line at ~15126 cm^{-1}.

2.2. Calibration aspects

(A) Extinction coefficients

In order to measure absolute extinction coefficients (in [cm^{-1}]) with FT-IBBCEAS, the broadband mirror reflectivity must be known. The mirror reflectivity was calibrated by filling a well evacuated cavity (P < 10^{-3} mbar) with a known amount of CO_2 (purity > 99.9%) at a pressure of ~6 mbar [40,41]. The reflectivity was then determined from the measured CO_2 extinction coefficients using the HITRAN absorption cross-sections of CO_2 in the wavenumber region between 14200 and 15600 cm^{-1} [1]. The reflectivity was found to be R = 0.9975 ± 0.0002 between 14975 cm^{-1} and 15275 cm^{-1}. The uncertainty of the reflectivity represents the largest contribution (~10%) to the systematic error of the measured water isotopologue absorption coefficients. Other uncertainties arise from the pressure measurement (~5%) and from intensity fluctuations of the SC light source (~4%) [43]. The total systematic mean square uncertainty contributing to the measured absorption coefficients was estimated to be ~12%.

(B) Wavenumber scale

Wavenumber calibration of the FTS is crucially important when new line positions are reported. For the purpose of minimizing the error in line positions, spectra of the most abundant water isotopologue ($H_2^{16}O$, doubly distilled) were measured using FT-IBBCEAS in the region between 14200 and 15600 cm^{-1}. The H_2O vapor was filled into the optical cavity at a pressure of 7.1 mbar. The wavenumber accuracy was evaluated by comparing the line positions of 30 measured isolated ro-vibrational lines with reasonable intensities $S(\lambda)$ to those in the Tomsk database in the region from 15250 to 15380 cm^{-1} (see Table 1), which is adjacent to the region where the ν_2+4ν_3 bands of $HD^{16}O$ and $HD^{18}O$ are located. Fig. 1 is essentially a graphical representation of **Table I**. The inset in Fig. 1 illustrates the excellent center wavenumber match between the measured FT-IBBCEAS spectrum (black trace) and the position from the Tomsk database, represented as a stick spectrum based on values for $S(\lambda)$. The average absolute discrepancy between the measured and literature line positions is 0.004 ± 0.002 cm^{-1}. This discrepancy is ~20 times smaller than the instrumental resolution of 0.08 cm^{-1}. We assume the reported wavenumber accuracy of $HD^{16}O$ and $HD^{18}O$ lines to be about 0.006 cm^{-1}. Therefore the wavenumber scale accuracy is sufficient to record accurate spectral line positions with a spectral resolution of 0.08 cm^{-1}.

2.3. Materials and gas preparations

$H_2^{18}O$ was purchased from Taiyo Nippon Sanso Corporation (purity > 98%) and the $D_2^{16}O$ was purchased from Sigma Aldrich (purity > 99.994%). The water samples were degassed by a sufficient number of "freeze pump-thaw" cycles before injection into the cavity. No further purification was applied. First the evacuated optical cavity was primed with $H_2^{18}O$ vapor at a pressure of ~4.0 mbar. Then $D_2^{16}O$ was injected (partial pressure ~4.0 mbar) to the chamber and left to equilibrate for ca. 16 h at room temperature. Hence the initial concentrations of $D_2^{16}O$ and $H_2^{18}O$ were approximately equal (50:50) before the commencement of deuterium exchange reactions. The total mixture pressure before the start of the actual measurement was observed to have reduced to ~7.7 mbar, probably due to adsorption on the cell wall surfaces.

3. Results and discussion

3.1. Spectral features in the region between 14975 cm^{-1} and 15275 cm^{-1}

Following the outlined preparation method (section 2.2), overview absorption spectra of the isotopologue mixture were recorded in the region between ~14200 and 15600 cm^{-1}. The spectra are dominated by ro-vibrational features of $H_2^{16}O$ and $H_2^{18}O$,

Table 1
Comparison of spectral line positions of $H_2^{16}O$ measured using FT-IBBCEAS and from the Tomsk database between 15254 and 15377 cm^{-1}.

FT-IBBCEAS ν_{exp} [cm^{-1}]	Tomsk database [35] ν_T [cm^{-1}]	Difference $\Delta\nu = \nu_T - \nu_{exp}$ [cm^{-1}]
15254.168	15254.168705	0.001
15268.345	15268.343544	−0.001
15277.189	15277.186536	−0.002
15280.910	15280.913667	0.004
15299.735	15299.738504	0.004
15308.330	15308.329864	0.000
15319.607	15319.610622	0.004
15324.157	15324.162458	0.005
15324.609	15324.616113	0.007
15325.408	15325.412676	0.005
15328.021	15328.016224	−0.005
15328.752	15328.746679	−0.005
15334.289	15334.294734	0.006
15334.477	15334.477784	0.001
15334.666	15334.673183	0.007
15335.170	15335.173524	0.004
15335.502	15335.506676	0.005
15336.202	15336.203029	0.001
15337.867	15337.871705	0.005
15341.106	15341.110478	0.004
15341.317	15341.323443	0.006
15341.528	15341.527176	−0.001
15342.959	15342.966593	0.008
15345.596	15345.598261	0.002
15346.613	15346.615950	0.003
15348.225	15348.224503	0.000
15351.427	15351.432081	0.005
15352.014	15352.019919	0.006
15362.259	15362.258558	0.000
15376.926	15376.920844	−0.005

however between 14975 and 15275 cm^{-1} strong lines of the ν_2+4ν_3 combination bands of $HD^{16}O$ and $HD^{18}O$ are clearly discernible. It turned out that this region is sufficiently isolated and exhibited merely weak interferences from $H_2^{16}O$ and $H_2^{18}O$ (see Fig. 2), thus allowing for ro-vibrational line assignments through comparison with the existing literature. Individual line assignments were established by comparing the measured $HD^{16}O$ and $HD^{18}O$ spectra with data reported in the Tomsk database. For that purpose, the line intensities of the two water isotopologues were calculated for the pertinent experimental conditions using the 'Tomsk' *abinito* variational database [35,46], and then visually inspected for recognizable patterns starting with the strongest ro-vibrational absorption features. In order to obtain unambiguous line-by-line assignments the cut off intensity for weaker lines was suitably adjusted for the spectral simulations using the Tomsk database. The minimal cut off intensities used were 10^{-29} cm/molecule and 10^{-32} cm/molecule for $HD^{16}O$ and $HD^{18}O$ respectively (note that the values in the database are weighted with the natural abundances of the different isotopologues).

Fig. 2 shows the measured absorption coefficients (Panel (a)) and the approximated absorption coefficient based on the (abundance-weighted) theoretical line intensities from the Tomsk database (Panel (b)) of the ν_2+4ν_3 bands of $HD^{16}O$ and $HD^{18}O$ between 14975 and 15275 cm^{-1}. As mentioned earlier, the ν_2+4ν_3 bands of the different isotopologues are not spectrally isolated. On the one hand, there are some discernable features of the isotoplogues $H_2^{16}O$ and $H_2^{18}O$ in the R branch of the $HD^{16}O$ ν_2+4ν_3 band, while the P branch appears less prone to those interferences (see Fig. 2a). On the other hand, the spectra of $HD^{16}O$ and $HD^{18}O$ are also not separated, however, rotational lines of both target isotopologues could nevertheless be readily distinguished.

After the assignment of individual lines (see Sections 3.2 and 3.3) the relative abundances of the four relevant isotopologues in

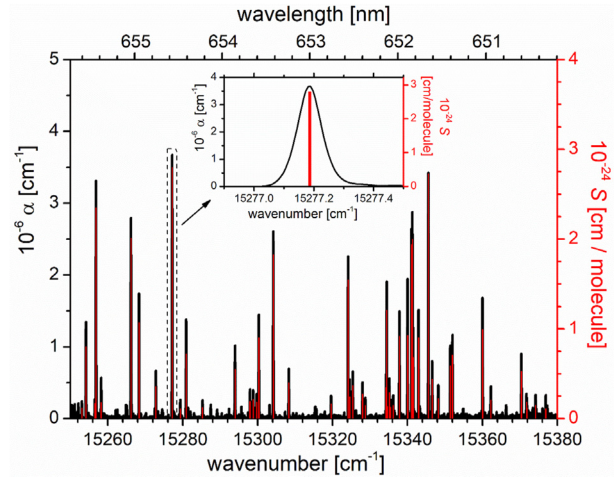

Fig. 1. Wavenumber calibration using the most abundant water isotopologue, $H_2^{16}O$. The black trace is the FT-IBBCEAS spectrum (left axis) of $H_2^{16}O$ at 7.1 mbar in the region from 15250 to 15380 cm^{-1} measured at a resolution of 0.08 cm^{-1}. The red trace represents the line positions and absorption strength, *S*, of $H_2^{16}O$ as reported in the Tomsk database (right axis). The inset shows a magnified view of the line at 15277.2 cm^{-1} in the dashed rectangle. (For interpretation of the references to colour in this figure legend, the reader is referred to the web version of this article.)

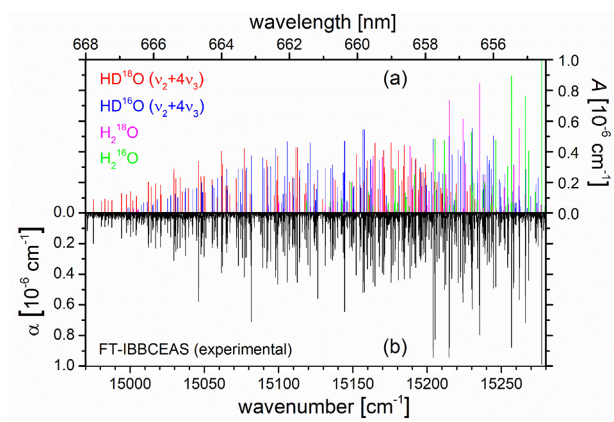

Fig. 2. (a) Upper panel: Stick spectrum of the ro-vibrational line absorption coefficient, $A = S_{Tomsk}$ [cm/molecule] / FWHM [cm^{-1}] / (natural relative abundance) × *n* [molecule cm^{-3}], of the ν_2+4ν_3 bands of $HD^{16}O$ (blue trace) and $HD^{18}O$ (red trace) from the Tomsk database [35] between 14970 and 15280 cm^{-1}, that best matches the measured spectrum. The magenta and green traces show the corresponding stick spectra of $H_2^{18}O$ and $H_2^{16}O$ in that region. Values of (natural relative abundance) × *n*: $HD^{16}O$ (3.10693×10^{-4}) × 6.7×10^{16} cm^{-3}, $HD^{18}O$ (6.23003×10^{-7}) × 5.5×10^{16} cm^{-3}, $H_2^{16}O$ (0.997317) × 3.8×10^{16} cm^{-3}, $H_2^{18}O$ (1.99983×10^{-3}) × 3.1×10^{16} cm^{-3}; FWHM = 0.1 cm^{-1}. The wavenumber scale of line intensities of $HD^{16}O$ was shifted by −0.361 cm^{-1} and the wavenumber scale of $H^{18}OD$ was shifted by −0.305 cm^{-1}. (b) Lower panel: main measured spectrum (absorption coefficient α, black trace) using FT-IBBCEAS. (For interpretation of the references to colour in this figure legend, the reader is referred to the web version of this article.)

the experiment were estimated by scaling the theoretical spectra [35] until a best match was found with the measured data as shown in Fig. 2 (see the figure caption for details). The partial pressures (and number densities) turned out to be ~2.20 mbar (≈5.5×10^{16} cm^{-3}) for $HD^{18}O$, ~2.68 mbar (≈6.7×10^{16} cm^{-3}) for $HD^{16}O$, ~1.24 mbar (≈3.1×10^{16} cm^{-3}) for $H_2^{18}O$, and ~1.52 mbar (≈3.8×10^{16} cm^{-3}) for $H_2^{16}O$. The sum of partial pressures agrees well with the overall pressure of 7.7 mbar after ^{18}O and D exchange (see previous section). The relative abundances of $HD^{18}O$, $HD^{16}O$, and $H_2^{18}O$ in the experiment were hence larger than their natural abundances by factors of ~462227, ~113, and ~81, respectively, while the abundance of $H_2^{16}O$ was reduced by a factor of ~5.

3.2. Ro-vibrational assignments for $HD^{16}O$

The $HD^{16}O$ ro-vibrational lines in the ν_2+4ν_3 band (014) were identified in comparison with the corresponding experimental line positions reported in Naumenko and Campargue [27], who used intracavity laser absorption spectroscopy to study $HD^{16}O$ at a resolution of 0.03 cm^{-1}, as well as with Bach et al. [28] who studied this isotopologue with a long path Fourier transform setup with a resolution of 0.06 cm^{-1}. (Note: Doppler FWHM at room temperature is ~0.05 cm^{-1}). In comparison with Ref. [27] and Ref. [28] the median absolute wavenumber discrepancy was merely ~0.010 cm^{-1} and ~0.008 cm^{-1}, respectively, which is approximately 10 times smaller than our instrumental spectral resolution. This good agreement of ~150 strong ro-vibrational lines (see column 3 of Table 2a) inspires confidence in our wavenumber calibration and at the same time corroborates the data in Refs. [27,28]. The assignment of the $HD^{16}O$ lines were then made on basis of the Tomsk database for our measurement conditions (see Table 2a). The large majority of lines in the Tomsk database was found to be systematically shifted to larger wavenumbers. An average absolute discrepancy of 0.361 ± 0.052 cm^{-1} (1σ) between the theoretical [35] and measured ν_2+4ν_3 line positions for $HD^{16}O$ was established. 141 assigned lines were also compared with the corresponding theoretical line list reported by Kyuberis et al. [9]. Here the absolute value of the median wavenumber discrepancy was again only ~0.008 cm^{-1} (see Table 2a). The fact that the wavenumber accuracy of the line positions of $HD^{16}O$ agrees really well with literature data implies the same can be expected for the line positions of $HD^{18}O$. In addition to lines from the ν_2+4ν_3 band of $HD^{16}O$, seven significantly strong lines from the overlapping ν_1+4ν_2+2ν_3 band were identified in the spectrum (see Table 2b). For this small number of lines, the average absolute discrepancy with regard to the Tomsk database was systematically less than half on average, i.e. 0.160 ± 0.036 cm^{-1} (1σ, student *t*-distribution assumed for small sample size). Several more line observations and alternative (ambiguous) assignments are listed in the supplementary material.

3.3. Ro-vibrational assignments for $HD^{18}O$

The instrument's well calibrated wavenumber scale with an overall uncertainty of 0.006 cm^{-1} (using $H_2^{16}O$ lines, see Section 2.1) and the good match with $HD^{16}O$ line position data from Refs. [9,28] enabled the assignment of $HD^{18}O$ lines on basis of the Tomsk database, using characteristic intensity patterns of the lines. 114 new ro-vibrational lines in the ν_2+4ν_3 band were identified and assigned for $HD^{18}O$; they are listed in Table 3a. The lower and upper rotational quantum numbers ($J\,K_a\,K_c$) are given for each rotational line; the assignments in Table 3a are taken from Ref. [35]. As in the case of $HD^{16}O$, the line positions for $HD^{18}O$ from the Tomsk database [35] were systematically shifted to larger wavenumbers. The average discrepancy of experimental $HD^{18}O$ lines with the predicted line positions was observed to be ~0.305 ± 0.064 cm^{-1} (1σ). In the case of $HD^{18}O$, only three lines in the ν_1+4ν_2+2ν_3 band were unambiguously identified (see Table 3b), with observed systematic shifts of ca. 0.122 cm^{-1}. Even though this latter systematic shift is rather uncertain due to the small sample size, the trend of a smaller systematic difference in the ν_1+4ν_2+2ν_3 combination band is the same as for $HD^{16}O$. It is interesting to note that the predictions from the Tomsk database appear to depend on two factors: (a) on the *vibrational mode* (mean shifts of 0.361 cm^{-1} for (014) versus 0.160 cm^{-1} for (142) in $HD^{16}O$), and (b) on the *relevant isotopologue* (shifts of 0.361 cm^{-1} and 0.160 cm^{-1} for $HD^{16}O$ versus 0.305 cm^{-1} and 0.122 cm^{-1} for $HD^{18}O$)), see also the captions of Tables 2 and 3).

It was also observed that the shifts are not symmetrically distributed around the stated average, which is also implied by the significant difference between the median and the mean in the observed shifts (see Figs. S1 and S2 in the supplementary material). The median may be a better measure for the expected discrepancy.

Fig. 3 shows a magnified view of the ν_2+4ν_3 band's P branch, i.e. the region between 15060 and 15080 cm^{-1}. The measured spectrum is compared with the line intensities from the Tomsk database after the latter were shifted by the average values of −0.305 cm^{-1} for $HD^{18}O$ and −0.361 cm^{-1} for $HD^{16}O$ (Tables 2a and 3a). The inset in Fig. 3 illustrates the quality of the match of center wavenumbers of lines after the shift of all lines by an average value. The dashed line in the inset shows an example of the good match with the data by Naumenko and Campargue [27], as well as Bach et al. [28] (see also Table 2a). The lines of the P branch of $HD^{16}O$ start at 14998.5 cm^{-1} and the lines of R branch ends at 15274.7 cm^{-1}, whereas the lines of the P branch of $HD^{18}O$ start at 14975.3 cm^{-1} and those of the R branch end at 15243.3 cm^{-1}. The P branch portion for Fig. 3 was selected in such a way that the line assignments of both $HD^{16}O$ and $HD^{18}O$ are clearly discernable (see the inset in Fig. 3).

Finally, it is worth noting that the spectral region studied here (14975–15275 cm^{-1} corresponding to the wavelength range of 654.7–667.8 nm) is highly relevant for NO_3 detection by spectroscopic methods, which use the origin of the strong B E′(0 0 0 0) ← X A_2′(0 0 0 0) transition of NO_3 with maximum at ~662 nm. In this region, water vapor is known to be the most important interfering species in the measurement and retrieval of NO_3 mixing ratios in ambient air samples. In "single wavelength" cavity ring-down approaches the position and absorption strength of lines is important and should be avoided or taken into account [47]. In broadband cavity enhanced absorption approaches to multiple absorber retrieval [39], small errors in modelling the water absorption can mask the NO_3 absorption features and lead to spurious NO_3 signals [48,49]. Thus the accurate knowledge of the position and absorption strength of even the less abundant water isotopologues, such as $HD^{16}O$ and $HD^{18}O$, may contribute to accurate quantitative retrieval procedures.

4. Conclusions

In this publication, the first observation of the ν_2+4ν_3 combination band of $HD^{18}O$ is reported using FT-IBBCEAS, illustrating the high suitability of this method for measurements of trace species isotopologues for which small sample volumes and high absorption sensitivity are required. 114 strong ro-vibrational lines for $HD^{18}O$ were assigned in the region between 14975.3 and 15243.3 cm^{-1} in comparison with line intensities and positions from the Tomsk database. The ν_2+4ν_3 band of $HD^{16}O$ has also been observed and fully agree with the results published by Naumenko and Camargue [27], Bach et al. [28], and Kyuberis et al. [9]. 141 strong lines were assigned for $HD^{16}O$ in the region between 15058.8 cm^{-1} and 15274.7 cm^{-1}. Systematic discrepancies in the line positions of 0.361 ± 0.052 cm^{-1} (1σ) and of 0.305 ± 0.064 cm^{-1} (1σ) were found for $HD^{16}O$ and $HD^{18}O$ respectively, in comparison with the Tomsk database. The presented data may be useful for future detection of atmospheric $HD^{16}O$ and $HD^{18}O$ in remote sensing applications. More high-resolution measurements of the ν_2+4ν_3 combination bands of these water isotopologues as well as new theoretical modelling of data in this spectral region are merited by this study.

Table 2a
Measured rotational line positions (col 1) in the vibrational transition (014) ← (000) of **HD^{16}O**, which were assigned on basis of positions in the Tomsk database [35] (col 2) are compared with reported experimental line positions [27,28] (col 3 & 4), and theoretical line lists [9] (col 5). The assignments (col 10, 11) are established by comparing the measured spectra with the theoretical line intensities from the 'Tomsk' database. The average difference of the measured (col 1) and predicted line positions from the Tomsk database [35] (col 2) is 0.361 ± 0.052 cm^{-1} (1σ) – Median 0.381 cm^{-1} (min. 0.170 cm^{-1}, max. 0.425 cm^{-1}). The differences, Δν, between the experimental data in this work and theoretical/measured line positions are listed in col 6–9. In total 141 ro-vibrational (014) lines were confirmed. Rotational quantum number assignments in *italics* are ambiguous in [35]: lines at 15119.696 and 15123.839 cm^{-1}, 15181.286 and 15185.994 cm^{-1}, 15195.516 and 15199.667 cm^{-1}, 15208.043, 15210.717 and 15214.092 cm^{-1}.

HD^{16}O FT-IBBCEAS	Tomsk data [35]	Ref. [27]	Ref. [28]	Ref. [9]	Difference (Δν)				Rotat. quantum number [35]	
ν_{exp} [cm^{-1}]	ν_T [cm^{-1}]	ν_N [cm^{-1}]	ν_B [cm^{-1}]	ν_K [cm^{-1}]	$\nu_T-\nu_{exp}$ [cm^{-1}]	$\nu_N-\nu_{exp}$ [cm^{-1}]	$\nu_B-\nu_{exp}$ [cm^{-1}]	$\nu_K-\nu_{exp}$ [cm^{-1}]	Upper (J K_a K_c)	Lower (J K_a K_c)
14980.652	–	–	14980.6566	–	–	–	0.005	–	–	–
14998.460	14998.790640	14998.482	14998.4526	14998.445948	0.331	0.022	−0.007	−0.014	(919)	(10010)[a]
14998.595	14998.859730	14998.482	14998.5781	14998.588736	0.265	−0.113	−0.017	−0.006	(744)	(845)[a]
14999.288	14999.643670	14999.278	14999.2604	14999.259860	0.356	−0.010	−0.028	−0.028	(835)	(936)
15007.763	15008.142890	15007.750	15007.7492	15007.750207	0.380	−0.013	−0.014	−0.013	(826)	(927)
15009.036	15009.440770	15009.080	15009.0553	15009.055569	0.405	0.044	0.019	0.020	(827)	(928)
15009.812	–	–	15009.8058	–	–	–	−0.006	–	–	–
15011.560	15011.956180	15011.573	15011.5664	15011.566883	0.397	0.013	0.006	0.007	(817)	(918)
15015.206	15015.573510	15015.223	15015.2195	15015.211553	0.368	0.017	0.014	0.006	(642)	(743)
15015.552	15015.882190	15015.494	15015.5701	15015.492908	0.330	−0.058	0.018	−0.059	(734)	(835)
15018.151	15018.495480	15018.137	15018.1408	15018.140773	0.344	−0.014	−0.010	−0.010	(808)	(909)
15018.309	15018.661020	15018.279	15018.2877	15018.287719	0.352	−0.030	−0.021	−0.021	(818)	(919)
15025.187	15025.567510	15025.156	15025.1710	15025.170528	0.381	−0.031	−0.016	−0.016	(725)	(826)
15027.311	15027.691500	15027.297	15027.3017	15027.301748	0.381	−0.014	−0.009	−0.009	(726)	(827)
15030.302	15030.682620	15030.288	15030.2877	15030.287709	0.381	−0.014	−0.014	−0.014	(716)	(817)
15031.854	15032.231200	15031.862	15031.8481	15031.840302	0.377	0.008	−0.006	−0.014	(633)	(734)
15032.223	15032.615690	15032.240	15032.2228	15032.222510	0.393	0.017	0.000	0.000	(634)	(735)
15036.938	15037.272430	15036.922	15036.9230	15036.923018	0.334	−0.016	−0.015	−0.015	(707)	(808)
15037.210	15037.582210	15037.202	15037.2007	15037.200696	0.372	−0.008	−0.009	−0.009	(717)	(818)
15042.099	15042.487830	15042.096	15042.0904	15042.090184	0.389	−0.003	−0.009	−0.009	(624)	(725)
15044.803	15045.180270	15044.806	15044.7972	15044.797231	0.377	0.003	−0.006	−0.006	(625)	(726)
15048.072	15048.464640	15048.065	15048.0650	15048.065029	0.393	−0.007	−0.007	−0.007	(615)	(716)
15048.471	15048.863090	15048.468	15048.4724	15048.472464	0.392	−0.003	0.001	0.001	(532)	(633)
15048.946	15049.321790	15048.933	15048.9295	15048.929423	0.376	−0.013	−0.017	−0.017	(533)	(634)
15055.462	15055.834340	15055.459	15055.4577	15055.457843	0.372	−0.003	−0.004	−0.004	(616)	(717)
15056.517	15056.881050	15056.506	15056.5045	15056.504454	0.364	−0.011	−0.013	−0.013	(606)	(707)
15058.792	15059.181610	15058.780	15058.7814	15058.781397	0.390	−0.012	−0.011	−0.011	(523)	(624)
15061.873	15062.257800	15061.861	15061.8620	15061.861994	0.385	−0.012	−0.011	−0.011	(524)	(625)
15065.067	15065.458120	15065.055	15065.0558	15065.055815	0.391	−0.012	−0.011	−0.011	(514)	(615)
15065.195	15065.580410	15065.194	15065.1888	15065.188531	0.385	−0.001	−0.006	−0.006	(431)	(532)
15065.496	15065.881820	15065.496	15065.4902	15065.490114	0.386	0.000	−0.006	−0.006	(432)	(533)
15072.133	15072.381000	15072.114	15072.1184	15072.119566	0.248	−0.019	−0.015	−0.013	(505)	(616)[a]
15072.871	15073.239710	15072.862	15072.8711	15072.876602	0.369	−0.009	0.000	−0.006	(515)	(616)
15074.453	15074.681280	15074.434	15074.4247	15074.420511	0.228	−0.019	−0.028	−0.032	(505)	(606)[a]
15075.176	15075.540000	15075.166	15075.1775	15075.177547	0.364	−0.010	0.002	0.002	(515)	(606)
15075.605	15075.999520	15075.583	15075.5992	15075.599196	0.395	−0.022	−0.006	−0.006	(422)	(523)
15078.415	15078.804000	15078.397	15078.4061	15078.405628	0.389	−0.018	−0.009	−0.009	(423)	(524)
15080.457	–	15080.473	15080.4797	–	–	0.016	0.023	–	–	–
15081.572[b]	15081.997230	15081.594	15081.5937	15081.593588	0.425	0.022	0.022	0.022	(413)	(514)
15081.805	15082.179800	15081.788	15081.7874	15081.793278	0.375	−0.017	−0.018	−0.012	(330)	(431)
15081.926	15082.305390	15081.918	15081.9134	15081.913512	0.380	−0.008	−0.013	−0.012	(331)	(432)
15089.300	15089.668880	15089.281	15089.2947	15089.294702	0.369	−0.019	−0.005	−0.005	(414)	(515)
15090.280	15090.554910	15090.266	15090.2736	15090.275102	0.275	−0.014	−0.006	−0.005	(404)	(505)
15092.585	15092.982560	15092.586	15092.5814	15092.581376	0.398	0.001	−0.004	−0.004	(321)	(422)
15093.202	15093.586700	15093.218	15093.2152	15093.213371	0.384	0.016	0.013	0.011	(414)	(505)
15093.346	–	15093.363	15093.3554	–		0.017	0.009	–	–	–
15094.641	15095.040630	15094.637	15094.6406	15094.640611	0.400	−0.004	0.000	0.000	(322)	(423)
15097.986	15098.378760	15097.978	15097.9775	15097.976957	0.393	−0.008	−0.009	−0.009	(312)	(413)

(*continued on next page*)

Table 2a (*continued*)

$HD^{16}O$ FT-IBBCEAS ν_{exp} [cm^{-1}]	Tomsk data [35] ν_T [cm^{-1}]	Ref. [27] ν_N [cm^{-1}]	Ref. [28] ν_B [cm^{-1}]	Ref. [9] ν_K [cm^{-1}]	Difference ($\Delta\nu$) $\nu_T - \nu_{exp}$ [cm^{-1}]	$\nu_N - \nu_{exp}$ [cm^{-1}]	$\nu_B - \nu_{exp}$ [cm^{-1}]	$\nu_K - \nu_{exp}$ [cm^{-1}]	Rotat. quantum number [35] Upper (J K_a K_c)	Lower (J K_a K_c)
15102.114	15102.471570	15102.102	15102.1156	15102.115612	0.358	−0.012	0.002	0.002	(651)	(652)
15103.010	15103.357300	15102.994	15103.0050	15103.004996	0.347	−0.016	−0.005	−0.005	(550)	(551)
15104.058	15104.342950	15104.052	15104.0576	15104.057634	0.285	−0.006	0.000	0.000	(303)	(404)
15105.828	15106.191490	15105.820	15105.8238	15105.824014	0.363	−0.008	−0.004	−0.004	(313)	(414)
15109.557	15109.957320	15109.547	15109.5561	15109.555874	0.400	−0.010	−0.001	−0.001	(220)	(321)
15110.122	15110.291750	15110.095	15110.1077	15110.108073	0.170	−0.027	−0.014	−0.014	(303)	(404)[a]
15110.664	15111.061780	15110.648	15110.6608	15110.660300	0.398	−0.016	−0.003	−0.004	(221)	(322)
15114.160	15114.484830	15114.146	15114.1585	15114.158502	0.325	−0.014	−0.002	−0.002	(211)	(312)
15119.696	15120.019930	15119.677	15119.6860	15119.686170	0.324	−0.019	−0.010	−0.010	*(202)*	*(303)*
15121.165	15121.556270	15121.153	15121.1586	15121.158813	0.391	−0.012	−0.006	−0.006	(212)	(313)
15123.440	15123.820880	15123.416	15123.4126	15123.411133	0.381	−0.024	−0.027	−0.029	(744)	(743)
15123.839	15124.052470	15123.842	15123.8368	15123.836834	0.213	0.003	0.002	0.002	*(202)*	*(303)*[a]
15124.615	15124.962390	15124.611	15124.6047	15124.592201	0.347	−0.004	−0.010	−0.023	(643)	(642)
15124.916	15125.300340	15124.934	15124.9264	15124.930879	0.384	0.018	0.010	0.015	(642)	(643)
15125.293	–	15125.336	15125.3195	–	–	0.043	0.027	–	(844)	(845)[f]
15125.542	15125.876190	15125.512	15125.5073	15125.507300	0.334	−0.030	−0.035	−0.035	(542)	(541)
15126.318	15126.681750	15126.315	15126.3116	15126.311567	0.364	−0.003	−0.006	−0.006	(441)	(440)
15126.318	15126.689670	15126.315	15126.3116	15126.311757	0.372	−0.003	−0.006	−0.006	(440)	(441)
15131.387	15131.787380	15131.382	15131.3956	15131.395406	0.400	−0.005	0.009	0.008	(110)	(211)
15135.094	15135.438670	15135.093	15135.0913	15135.091320	0.345	−0.001	−0.003	−0.003	(101)	(202)
15136.186	15136.576060	15136.175	15136.1743	15136.174152	0.390	−0.011	−0.012	−0.012	(111)	(212)
15139.478	15139.862690	15139.461	15139.4636	15139.463578	0.385	−0.017	−0.014	−0.014	(634)	(633)
15139.824	15140.046990	15139.822	15139.8194	15139.819359	0.223	−0.002	−0.005	−0.005	(101)	(202)[a]
15142.047	15142.431940	15142.037	15142.0333	15142.033990	0.386	−0.010	−0.014	−0.013	(533)	(532)
15143.485	15143.875120	15143.495	15143.4788	15143.478515	0.390	0.010	−0.006	−0.006	(432)	(431)
15144.118	15144.508380	15144.123	15144.1114	15144.111260	0.390	0.005	−0.007	−0.007	(431)	(432)
15144.442	15144.745440	15144.363	15144.3495	15144.349492	0.303	−0.079	−0.093	−0.093	(331)	(330)
15144.442	15144.837660	15144.461	15144.4470	15144.446990	0.396	0.019	0.005	0.005	(330)	(331)
15145.753	15146.114200	15145.758	15145.7455	15145.744928	0.362	0.005	−0.008	−0.008	(313)	(312)
15145.903	–	–	15145.9828	–		–	0.080	–	–	–
15146.318	15146.686820	15146.298	15146.2873	15146.287805	0.369	−0.020	−0.031	−0.030	(633)	(634)
15150.212	15150.607810	15150.207	15150.2060	15150.205991	0.396	−0.005	−0.006	−0.006	(423)	(422)
15150.604	15150.950230	15150.596	15150.5963	15150.596300	0.346	−0.008	−0.008	−0.008	(000)	(101)
15154.620	15155.021060	15154.620	15154.6179	15154.617859	0.401	0.000	−0.002	−0.002	(322)	(321)
15155.380	15155.764370	15155.373	15155.3679	15155.365222	0.384	−0.007	−0.012	−0.015	(212)	(211)
15156.781	15157.184420	15156.785	15156.7802	15156.780221	0.403	0.004	−0.001	−0.001	(221)	(220)
15157.708	15158.098960	15157.699	15157.6943	15157.694327	0.391	−0.009	−0.014	−0.014	(220)	(221)
15159.033	15159.434240	15159.033	15159.0285	15159.028529	0.401	0.000	−0.005	−0.004	(321)	(322)
15161.813	15162.207960	15161.803	15161.8046	15161.804654	0.395	−0.010	−0.008	−0.008	(111)	(110)
15162.551	15162.958630	15162.538	15162.5517	15162.552054	0.408	−0.013	0.001	0.001	(422)	(423)
15167.779	15168.165560	15167.770	15167.7713	15167.771345	0.387	−0.009	−0.008	−0.008	(110)	(111)
15172.495	15172.822850	15172.486	15172.4928	15172.492971	0.328	−0.009	−0.002	−0.002	(211)	(212)
15181.286	15181.614410	15181.276	15181.2646	15181.264431	0.328	−0.010	−0.021	−0.022	*(101)*	*(000)*
15185.994	15186.222730	15185.997	15185.9923	15185.992470	0.229	0.003	−0.002	−0.002	*(101)*	*(000)*[a]
15191.742	15192.142550	15191.739	15191.7412	15191.741161	0.401	−0.003	−0.001	−0.001	(212)	(111)
15195.516	15195.846050	15195.495	15195.5083	15195.508219	0.330	−0.021	−0.008	−0.008	*(202)*	*(101)*
15198.122	15198.454760	15198.114	15198.1242	15198.123473	0.333	−0.008	0.002	0.001	(211)	(110)
15199.667	15199.878590	15199.653	15199.6590	15199.658883	0.212	−0.014	−0.008	−0.008	*(202)*	*(101)*[a]
15202.755	15203.162700	15202.751	15202.7563	15202.756312	0.408	−0.004	0.001	0.001	(322)	(221)
15204.066	15204.452220	15204.082	15204.0796	15204.079397	0.386	0.016	0.014	0.013	(313)	(212)
15205.151	15205.556880	15205.157	15205.1481	15205.148450	0.406	0.006	−0.003	−0.003	(321)	(220)
15206.137	15206.532990	15206.132	15206.1319	15206.132227	0.396	−0.005	−0.005	−0.005	(432)	(331)
15208.043	15208.331350	15208.039	15208.0410	15208.040832	0.288	−0.004	−0.002	−0.002	*(303)*	*(202)*
15210.055	–	15210.035	15209.8779	–	–	−0.020	−0.177	–	(753)	(652)[f]

Table 2a (*continued*)

$HD^{16}O$ FT-IBBCEAS	Tomsk data [35]	Ref. [27]	Ref. [28]	Ref. [9]	Difference ($\Delta\nu$)				Rotat. quantum number [35]	
ν_{exp} [cm^{-1}]	ν_T [cm^{-1}]	ν_N [cm^{-1}]	ν_B [cm^{-1}]	ν_K [cm^{-1}]	$\nu_T - \nu_{exp}$ [cm^{-1}]	$\nu_N - \nu_{exp}$ [cm^{-1}]	$\nu_B - \nu_{exp}$ [cm^{-1}]	$\nu_K - \nu_{exp}$ [cm^{-1}]	Upper ($J\ K_a\ K_c$)	Lower ($J\ K_a\ K_c$)
15210.717	15210.941370	15210.720	15210.7219	15210.722149	0.224	0.003	0.005	0.005	*(303)*	*(202)*[a]
15214.092	15214.280150	15214.093	15214.0913	15214.091271	0.188	0.001	−0.001	−0.001	*(303)*	*(202)*[a]
15214.778	15215.149530	15214.778	15214.7726	15214.768682	0.372	0.000	−0.005	−0.009	(414)	(313)
15216.653	15217.059490	15216.646	15216.6529	15216.653144	0.406	−0.007	0.000	0.000	(423)	(322)
15218.310	15218.696800	15218.312	15218.3201	15218.320118	0.386	0.002	0.010	0.010	(643)	(542)
15220.917	15221.177070	15220.885	15220.8915	15220.891067	0.260	−0.032	−0.026	−0.026	(404)	(303)
15222.514	15222.939060	15222.505	15222.5321	15222.529302	0.425	−0.009	0.018	0.015	(422)	(321)
15224.367	15224.622410	15224.343	15224.3530	15224.352995	0.255	−0.024	−0.014	−0.014	(505)	(414)[a]
15224.789	15225.113050	15224.760	15224.7656	15224.758722	0.324	−0.029	−0.023	−0.030	(854)	(753)
15225.113	15225.481130	15225.108	15225.1104	15225.110031	0.368	−0.005	−0.003	−0.003	(515)	(414)
15228.887	–	15228.898	15228.9024	–	–	0.011	0.015	–	(625)	(606)[f]
15229.693	15230.100870	15229.690	15229.6956	15229.695612	0.408	−0.003	0.003	0.003	(524)	(423)
15230.364	15230.780240	15230.352	15230.3681	15230.368493	0.416	−0.012	0.004	0.004	(413)	(312)
15230.574	15230.847210	15230.564	15230.5777	15230.578949	0.273	−0.010	0.004	0.005	(505)	(404)[a]
15233.143	15233.547710	15233.116	15233.1304	15233.130459	0.405	−0.027	−0.013	−0.013	(744)	(643)
15233.806	15234.187300	15233.782	15233.8007	15233.801028	0.381	−0.024	−0.005	−0.005	(606)	(515)
15234.032	15234.424370	15234.011	15234.0341	15234.038611	0.392	−0.021	0.002	0.007	(616)	(515)
15235.471	15235.866970	15235.450	15235.4610	15235.461313	0.396	−0.021	−0.010	−0.010	(634)	(533)
15237.723	15238.105120	15237.724	15237.7196	15237.719697	0.382	0.001	−0.003	−0.003	(606)	(505)
15237.957[c]	15238.342190	15237.959	15237.9573	15237.957280	0.385	0.002	0.000	0.000	(616)	(505)
15239.403	15239.796960	15239.408	15239.3902	15239.392372	0.394	0.005	−0.013	−0.011	(633)	(532)
15240.495	15240.905830	15240.507	15240.4945	15240.494258	0.411	0.012	−0.001	−0.001	(523)	(422)
15241.595	15241.981800	15241.599	15241.5881	15241.588073	0.387	0.004	−0.007	−0.007	(625)	(524)
15241.799	15242.184180	15241.807	15241.7921	15241.792162	0.385	0.008	−0.007	−0.007	(717)	(616)
15243.132	15243.483550	15243.134	15243.1244	15243.124062	0.352	0.002	−0.008	−0.008	(707)	(606)
15244.578	15244.991000	15244.585	15244.5795	15244.579491	0.413	0.007	0.002	0.001	(514)	(413)
15248.639	15249.018050	15248.632	15248.6330	15248.632994	0.379	−0.007	−0.006	−0.006	(818)	(717)
15248.827	–	15248.800	15248.8029	–	–	−0.027	−0.024	–	(1019)	(10110)[f]
15249.414	15249.773630	15249.404	15249.4071	15249.407455	0.360	−0.010	−0.007	−0.007	(808)	(707)
15249.686	15250.007450	15249.670	15249.6676	15249.667657	0.321	−0.016	−0.018	−0.018	(735)	(634)
15249.927	15250.301830	15249.916	15249.9188	15249.917188	0.375	−0.011	−0.008	−0.010	(818)	(707)
15252.375	15252.774300	15252.374	15252.3727	15252.372695	0.399	−0.001	−0.002	−0.002	(726)	(625)
15254.507	15254.874770	15254.499	15254.5008	15254.498377	0.368	−0.008	−0.006	−0.009	(909)	(818)[a]
15256.857[d]	15257.156160	15256.743	15256.7465	15256.746421	0.299	−0.114	−0.111	−0.111	(615)	(514)
15257.633	15258.029670	15257.619	15257.6246	15257.624617	0.397	−0.014	−0.008	−0.008	(734)	(633)
15258.258[e]	15258.629280	15258.213	15258.2185	15258.218845	0.371	−0.045	−0.040	−0.039	(624)	(523)
15259.162	15259.479270	15259.132	15259.1391	15259.139193	0.317	−0.030	−0.023	−0.023	(10110)	(919)[a]
15259.516	15259.858860	15259.497	15259.5049	15259.501958	0.343	−0.019	−0.011	−0.014	(10010)	(919)[a]
15259.870	15260.221510	15259.856	15259.8644	15259.864745	0.351	−0.014	−0.006	−0.005	(10010)	(909)[a]
15261.723	15262.123640	15261.714	15261.7265	15261.725505	0.401	−0.009	0.004	0.003	(827)	(726)
15262.288	15262.583520	15262.281	15262.2884	15262.299987	0.295	−0.007	0.000	0.012	(836)	(735)
15263.049	15263.397670	15263.088	15263.0906	15263.090585	0.349	0.039	0.042	0.042	(11111)	(10110)[a]
15266.349	15266.749240	15266.347	15266.3437	15266.343575	0.400	−0.002	−0.005	−0.005	(716)	(615)
15267.464	15267.825700	15267.446	15267.4435	15267.443558	0.362	−0.018	−0.021	−0.020	(945)	(844)
15269.739	15270.119200	15269.723	15269.7243	15269.724214	0.381	−0.016	−0.015	−0.015	(928)	(827)
15273.392	15273.785090	15273.382	15273.3848	15273.384311	0.393	−0.010	−0.007	−0.008	(817)	(716)
15273.950	15274.341470	15273.956	15273.9586	15273.958611	0.392	0.006	0.009	0.009	(937)	(836)
15274.718	15275.121000	15274.715	15274.7098	15274.710160	0.403	−0.003	−0.008	−0.008	(725)	(624)

[a] Lines have an alternative assignment in Ref. [9] – also see Table in the supplementary material.
[b] Experimental line (at 15081.572 cm^{-1}) is also listed in Table 3a, since a $HD^{16}O$ line and a $HD^{18}O$ line from Ref. [35] overlap at this position within the experimental resolution.
[c] Experimental line (at 15237.957 cm^{-1}) overlaps with a $H_2^{18}O$ line predicted in the Tomsk database [35].
[d] Experimental line (at 15256.857 cm^{-1}) overlaps with a $H_2^{16}O$ line from the Tomsk database [35].
[e] Experimental line (at 15258.258 cm^{-1}) overlaps with a $H_2^{18}O$ and a $H_2^{16}O$ absorption line [35].
[f] Assignments from Naumenko and Campargue [27].

Table 2b
Measured rotational line positions (col 1) in the vibrational transition (142) ← (000) of **$HD^{16}O$**, which were assigned on basis of positions in the Tomsk database [35] (col 2) are compared with reported experimental line positions [27,28] (col 3 & 4), and theoretical line lists [9] (col 5). The assignments (col 10, 11) are established by comparing the measured spectra with the theoretical line intensities from the 'Tomsk' database. The average difference of the measured (col 1) and predicted line positions from the Tomsk database [35] (col 2) is 0.160 ± 0.036 cm^{-1} (1σ, Student's *t*-distribution assumed) – Median 0.153 cm^{-1} (min. 0.109 cm^{-1}, max. 0.203 cm^{-1}). The differences, Δν, between the experimental data in this work and theoretical/measured line positions are listed in col (6–9). In total 9 ro-vibrational (142) lines were confirmed.

$HD^{16}O$ FT-IBBCEAS	Tomsk data [35]	Ref. [27]	Ref. [28]	Ref. [9]	Difference (Δν)				Rotat. Quantum number [35]	
ν_{exp} [cm^{-1}]	ν_T [cm^{-1}]	ν_N [cm^{-1}]	ν_B [cm^{-1}]	ν_K [cm^{-1}]	$\nu_T - \nu_{exp}$ [cm^{-1}]	$\nu_N - \nu_{exp}$ [cm^{-1}]	$\nu_B - \nu_{exp}$ [cm^{-1}]	$\nu_K - \nu_{exp}$ [cm^{-1}]	Upper (J K_a K_c)	Lower (J K_a K_c)
15041.760	15041.959390	15041.774	15041.7649	15041.764675	0.199	0.014	0.005	0.005	(707)	(808)
15080.246	–	15080.258	15080.2574	–	–	0.012	0.011	–	(505)	(606)[a]
15091.545	15091.713390	15091.550	15091.5528	15091.552977	0.168	0.005	0.008	0.008	(404)	(515)
15095.485	15095.631210	15095.468	15095.4736	15095.471646	0.146	−0.017	−0.011	−0.013	(404)	(505)
15217.053	15217.194040	15217.029	15217.0270	15217.026957	0.141	−0.024	−0.026	−0.026	(404)	(313)
15226.100	15226.253360	15226.086	15226.0876	15226.087611	0.153	−0.014	−0.012	−0.012	(404)	(303)
15236.428	15236.537110	15236.408	15236.4142	15236.414343	0.109	−0.020	−0.014	−0.014	(505)	(404)
15247.968	15248.170500	15247.958	15247.9657	15247.965719	0.203	−0.010	−0.002	−0.002	(707)	(606)
15267.629	–	15267.626	15267.6208	–	–	−0.003	−0.008	–	(11011)	(10110)[a]

[a] Assignments from Naumenko and Campargue [27].

Table 3a
Measured rotational line positions (col 2) in the vibrational transition (014) ← (000) of **$HD^{18}O$**. The vibrational and rotational quantum number assignments (col 5, 6) were established on basis of positions in the Tomsk database [35] (col 3). The differences, Δν, between the experimental data of this work (col 2) and those in the Tomsk database [35] (col 3) are listed in col 4. The average difference is 0.305 ± 0.064 cm^{-1} (1σ) – median 0.331 cm^{-1} (min. 0.130 cm^{-1}, max. 0.388 cm^{-1}). In total 114 ro-vibrational (014) lines were confirmed. Rotational quantum number assignments set in *italics* in rows 26/27, 32/33, 39/40, 63/64, 68/70 are ambiguous in [35].

#	$HD^{18}O$ FT-IBBCEAS [this work]	Tomsk database [35]	Difference (Δν)	Rotational quantum number [35]	
	ν_{exp} [cm^{-1}]	ν_T [cm^{-1}]	$\nu_T - \nu_{exp}$ [cm^{-1}]	Upper (J K_a K_c)	Lower (J K_a K_c)
1	14975.288	14975.597870	0.310	(808)	(909)
2	14980.652	14981.000310	0.348	(725)	(826)
3	14982.957	14983.299160	0.342	(726)	(827)
4	14985.247	14985.560670	0.314	(716)	(817)
5	14987.499	14987.846860	0.348	(633)	(734)
6	14987.657	14987.967100	0.310	(541)	(642)
7	14987.838	14988.188090	0.350	(634)	(735)
8	14994.113	14994.405230	0.292	(717)	(818)
9	14994.264	14994.570690	0.307	(707)	(808)
10	14997.450	14997.807970	0.358	(624)	(725)
11	15000.343	15000.695300	0.352	(625)	(726)
12	15001.963	15002.176370	0.213	(615)	(716)
13	15004.019	15004.349280	0.330	(532)	(633)
14	15004.464	15004.813060	0.349	(533)	(634)
15	15012.162	15012.459800	0.298	(616)	(717)
16	15012.479	15012.752540	0.274	(606)	(707)
17	15014.136	15014.484850	0.349	(523)	(624)
18	15017.209	15017.555650	0.347	(524)	(625)
19	15020.358	15020.629750	0.272	(514)	(615)
20	15020.614	15020.951350	0.337	(431)	(532)
21	15020.923	15021.261830	0.339	(432)	(533)
22	15029.488	15029.772960	0.285	(515)	(616)
23	15029.593	15029.913440	0.320	(505)	(606)
24	15030.761	15031.118450	0.357	(422)	(523)
25	15033.640	15033.986970	0.347	(423)	(524)
26	15035.213	15035.391430	0.178	*(413)*	*(514)*
27	15039.341	15039.485640	0.145	*(413)*	*(514)*
28	15046.106	15046.392600	0.287	(404)	(505)
29	15046.106	15046.415150	0.309	(414)	(515)
30	15047.658	15048.015380	0.357	(321)	(422)
31	15049.752	15050.110330	0.358	(322)	(423)
32	15051.025	15051.177940	0.153	*(312)*	*(413)*
33	15055.304	15055.496210	0.192	*(312)*	*(413)*
34	15058.551	15058.858850	0.308	(550)	(551)
35	15061.526	15061.857000	0.331	(303)	(404)
36	15062.197	15062.455150	0.258	(313)	(414)
37	15064.539	15064.899580	0.361	(220)	(321)
38	15065.662	15066.023750	0.362	(221)	(322)
39	15067.214	15067.374110	0.160	*(211)*	*(312)*
40	15071.583	15071.784630	0.202	*(211)*	*(312)*
41	15076.841	15077.178770	0.338	(202)	(303)

Table 3a (*continued*)

#	$HD^{18}O$ FT-IBBCEAS [this work]	Tomsk database [35]	Difference ($\Delta\nu$)	Rotational quantum number [35]	
	ν_{exp} [cm^{-1}]	ν_T [cm^{-1}]	$\nu_T - \nu_{exp}$ [cm^{-1}]	Upper ($J\ K_a\ K_c$)	Lower ($J\ K_a\ K_c$)
42	15077.737	15077.977960	0.241	(212)	(313)
43	15080.781	15081.094670	0.314	(542)	(541)
44	15080.781	15081.168660	0.388	(541)	(542)
45	15081.572[a]	15081.871860	0.300	(441)	(440)
46	15092.020	15092.366710	0.347	(101)	(202)
47	15092.803	15093.044860	0.242	(111)	(212)
48	15097.014	15097.364430	0.350	(533)	(532)
49	15098.461	15098.804090	0.343	(432)	(431)
50	15099.108	15099.460760	0.353	(431)	(432)
51	15099.334	15099.664130	0.330	(331)	(330)
52	15099.402	15099.759960	0.358	(330)	(331)
53	15099.545	15099.893250	0.348	(532)	(533)
54	15104.901	15105.252120	0.351	(423)	(422)
55	15107.365	15107.709570	0.345	(000)	(101)
56	15109.331	15109.696290	0.365	(322)	(321)
57	15111.515	15111.868530	0.354	(221)	(220)
58	15111.673	15111.907220	0.234	(212)	(211)
59	15112.442	15112.797820	0.356	(220)	(221)
60	15113.813	15114.176430	0.363	(321)	(322)
61	15117.399	15117.758820	0.360	(422)	(423)
62	15118.265	15118.494230	0.229	(111)	(110)
63	15119.892	15120.054670	0.163	*(110)*	*(111)*
64	15124.276	15124.488800	0.213	*(110)*	*(111)*
65	15129.655	15129.855110	0.200	(211)	(212)
66	15137.918	15138.267250	0.349	(101)	(000)
67	15147.862	15148.108060	0.246	(212)	(111)
68	15150.717	15150.893970	0.177	*(211)*	*(110)*
69	15152.186	15152.528470	0.342	(202)	(101)
70	15155.101	15155.304490	0.203	*(211)*	*(110)*
71	15157.233	15157.594530	0.362	(322)	(221)
72	15159.659	15160.021220	0.362	(321)	(220)
73	15159.802	15160.069930	0.268	(313)	(212)
74	15160.751	15161.111250	0.360	(432)	(331)
75	15161.195	15161.542470	0.347	(431)	(330)
76	15164.819	15165.150100	0.331	(303)	(202)
77	15167.169	15167.342040	0.173	(312)	(211)
78	15170.777	15171.055790	0.279	(414)	(313)
79	15171.056	15171.413180	0.357	(423)	(322)
80	15171.470	15171.660310	0.190	(312)	(211)
81	15175.523	15175.873830	0.351	(533)	(432)
82	15175.779	15176.095530	0.317	(404)	(303)
83	15177.007	15177.344780	0.338	(422)	(321)
84	15177.067[b]	15177.435510	0.369	(532)	(431)
85	15180.683	15180.977910	0.295	(515)	(414)
86	15183.139	15183.325560	0.187	(413)	(312)
87	15184.020	15184.371530	0.352	(524)	(423)
88	15184.631	15184.949840	0.319	(505)	(404)
89	15187.290	15187.419770	0.130	(413)	(312)
90	15189.512	15189.817040	0.305	(616)	(515)
91	15189.926	15190.281390	0.355	(634)	(533)
92	15192.367	15192.657680	0.291	(606)	(505)
93	15194.039	15194.391280	0.352	(633)	(532)
94	15194.966	15195.330180	0.364	(523)	(422)
95	15195.908	15196.264830	0.357	(625)	(524)
96	15197.271	15197.580400	0.309	(717)	(616)
97	15198.800	15199.082460	0.282	(514)	(413)
98	15198.981	15199.287810	0.307	(707)	(606)
99	15203.734	15204.084530	0.351	(735)	(634)
100	15204.066[c]	15204.334970	0.269	(818)	(717)
101	15204.887	15205.212040	0.325	(808)	(707)
102	15206.574	15206.939080	0.365	(726)	(625)
103	15209.316	15209.528370	0.212	(615)	(514)
104	15209.859[d]	15210.184250	0.325	(919)	(818)
105	15210.356	15210.685230	0.329	(909)	(808)
106	15212.299	15212.655620	0.357	(734)	(633)
107	15212.503	15212.872190	0.369	(624)	(523)
108	15213.362[e]	15213.507650	0.146	(615)	(514)
109	15215.817	15216.159430	0.342	(827)	(726)
110	15219.697	15220.010760	0.314	(716)	(615)
111	15226.921	15227.255310	0.334	(817)	(716)
112	15228.887[c]	15229.245090	0.358	(725)	(624)
113	15232.058	15232.392350	0.334	(918)	(817)
114	15243.283	15243.621020	0.338	(826)	(725)

[a] Experimental line 45 (at 15081.572 cm^{-1}) is also listed in Table 2a, since a HD^{16}O line and a HD^{18}O line from Ref. [35] overlap at this position within the resolution of the setup.
[b] Experimental line 84 (at 15177.067 cm^{-1}) overlaps with a $H_2^{18}O$ line predicted in the Tomsk database [35].
[c] Experimental line 100 (at 15204.066 cm^{-1}) overlaps with a $H_2^{18}O$ and HD^{16}O line from [35].
[d] Experimental lines 104 and 112 (at 15209.859 and 15228.887 cm^{-1}) overlap with individual HD^{16}O absorption lines reported in [28].
[e] Experimental line 108 (at 15213.362 cm^{-1}) overlaps with a HD^{16}O line reported in Refs. [9,28].

Table 3b
Measured rotational line positions (col 2) in the vibrational transition (142) ← (000) of **HD^{18}O**. The vibrational and rotational quantum number assignments (col 5, 6) were established on basis of positions in the Tomsk database [35] (col 3). The differences, Δν, between the experimental data (col 2) in this work and those in the Tomsk database [35] (col 3) are listed in col 4. The average difference is 0.122 cm^{-1}.

#	HD^{18}O FT-IBBCEAS [this work]	Tomsk database [35]	Difference (Δν)	Rotational quantum number [35]	
	ν_{exp} [cm^{-1}]	ν_T [cm^{-1}]	$\nu_T - \nu_{exp}$ [cm^{-1}]	Upper ($J\ K_a\ K_c$)	Lower ($J\ K_a\ K_c$)
1	15057.308	15057.423900	0.116	(313)	(414)
2	15073.097	15073.221850	0.125	(212)	(313)
3	15154.913	15155.038680	0.126	(313)	(212)

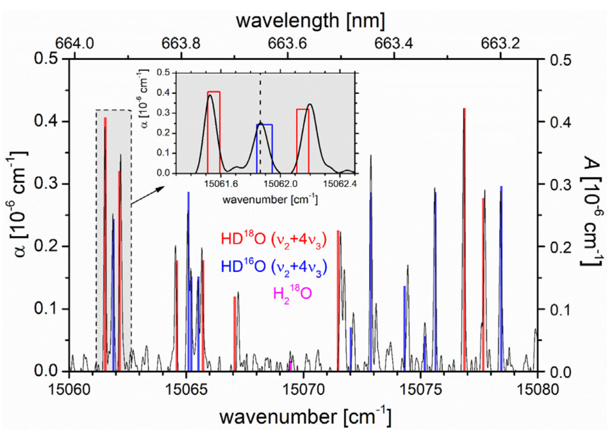

Fig. 3. Magnified view of Fig. 2; a section of the P branch of the ν_2+4ν_3 band of HD^{18}O and HD^{16}O. Black trace: measured FT-IBBCEAS spectrum. Red trace: line intensities of HD^{18}O. Blue trace: line intensities of HD^{16}O. ***Inset*** (the shaded region in the black dashed rectangle): magnified view of the region between 15061.3 cm^{-1} and 15062.5 cm^{-1}. The line at 15061.9 cm^{-1} belongs to HD^{16}O, whereas the other two peaks at 15061.5 cm^{-1} and 15062.2 cm^{-1} are assigned to HD^{18}O. The dashed vertical line in the inset indicates the position of the corresponding line listed in Refs. [27,28]. (For interpretation of the references to colour in this figure legend, the reader is referred to the web version of this article.)

CRediT authorship contribution statement

S. Chandran: Formal analysis, Writing - review & editing, Methodology. **S. Dixneuf:** Investigation, Data curation, Funding acquisition. **J. Orphal:** Conceptualization, Writing - review & editing. **A.A. Ruth:** Writing - original draft, Supervision, Conceptualization, Project administration.

Declaration of Competing Interest

The authors declare that they have no known competing financial interests or personal relationships that could have appeared to influence the work reported in this paper.

Acknowledgements

Support for an International Mobility Fellowships in Science, Engineering and Technology 2010 for S. Dixneuf, jointly awarded by the Irish Research Council for Science Research and Technology (IRCSET) and the FP7 Marie Curie INSPIRE programme, is gratefully acknowledged. This work has received funding from the European Union's Horizon 2020 research and innovation programme through the EUROCHAMP-2020 Infrastructure Activity under grant agreement No 730997. We also thank Prof J. Wenger of the School of Chemistry, UCC for his support, and Mr. C. Roche and Mr. J. Sheehan of the Physics Department for their excellent technical assistance.

Appendix A. Supplementary material

Supplementary data to this article can be found online at https://doi.org/10.1016/j.jms.2020.111395.

References

[1] I.E. Gordon, L.S. Rothman, C. Hill, R.V. Kochanov, Y. Tan, P.F. Bernath, M. Birk, V. Boudon, A. Campargue, K.V. Chance, B.J. Drouin, J.M. Flaud, R.R. Gamache, J.T. Hodges, D. Jacquemart, V.I. Perevalov, A. Perrin, K.P. Shine, M.A.H. Smith, J. Tennyson, G.C. Toon, H. Tran, V.G. Tyuterev, A. Barbe, A.G. Császár, V.M. Devi, T. Furtenbacher, J.J. Harrison, J.M. Hartmann, A. Jolly, T.J. Johnson, T. Karman, I. Kleiner, A.A. Kyuberis, J. Loos, O.M. Lyulin, S.T. Massie, S.N. Mikhailenko, N. Moazzen-Ahmadi, H.S.P. Müller, O.V. Naumenko, A.V. Nikitin, O.L. Polyansky, M. Rey, M. Rotger, S.W. Sharpe, K. Sung, E. Starikova, S.A. Tashkun, J.V. Auwera, G. Wagner, J. Wilzewski, P. Wcisło, S. Yu, E.J. Zak, The HITRAN2016 molecular spectroscopic database, J. Quant. Spectrosc. Radiat. Transf. 203 (2017) 3–69, https://doi.org/10.1016/j.jqsrt.2017.06.038.
[2] Z. Wei, X. Lee, F. Aemisegger, M. Marion Benetti, M. Berkelhammer, K. Casado, E. Caylor, C. Christner, O. Dyroff, Y. García, T. González, N. Griffis, J. Kurita, M.-C. Liang, G. Liang, D. Lin, K. Noone, N.C. Gribanov, M. Munksgaard, F. Schneider, H. C. Ritter, C. Steen-Larsen, X. Vallet-Coulomb, J.S. Wen, W. Wright, K. Yoshimura Xiao, A global database of water vapor isotopes measured with high temporal resolution infrared laser spectroscopy, Nature Sci. Data 6 (2019) 180302, https://doi.org/10.1038/sdata.2018.302.
[3] H. Partridge, D.W. Schwenke, The determination of an accurate isotope dependent potential energy surface for water from extensive ab initio calculations and experimental data, J. Chem. Phys. 106 (1997) 4618–4639, https://doi.org/10.1063/1.473987.
[4] S.N. Yurchenko, B.A. Voronin, R.N. Tolchenov, N. Doss, O.V. Naumenko, W. Thiel, J. Tennyson, Potential energy surface of HDO up to 25000 cm^{-1}, J. Chem. Phys. 128 (2008) 044312, https://doi.org/10.1063/1.2806165.
[5] J. Tennyson, P.F. Bernath, L.R. Brown, A. Campargue, A.G. Csaszar, L. Daumont, R.R. Gamache, J.T. Hodges, O.V. Naumenko, O.L. Polyansky, L.S. Rothman, R.A. Toth, A.C. Vandaele, N.F. Zobov, S. Fally, A.Z. Fazliev, T. Furtenbacher, I.E. Gordon, S.M. Hu, S.N. Mikhailenko, B.A. Voronin, IUPAC critical evaluation of the rotational-vibrational spectra of water vapor. Part II Energy levels and transition wavenumbers for HD^{16}O, (HD^{17}O, and HD^{18}O), J. Quant. Spectrosc. Radiat. Transf. 111 (2010) 2160–2184, https://doi.org/10.1016/j.jqsrt.2010.06.012.
[6] B.A. Voronin, J. Tennyson, R.N. Tolchenov, A.A. Lugovskoy, S.N. Yurchenko, A high accuracy computed line list for the HDO molecule, Mon. Not. R. Astron. Soc. 402 (2010) 492–496, https://doi.org/10.1111/j.1365-2966.2009.15904.x.

[7] J. Tennyson, P.F. Bernath, L.R. Brown, A. Campargue, A.G. Császár, L. Daumont, R.R. Gamache, J.T. Hodges, O.V. Naumenko, O.L. Polyansky, L.S. Rothman, A.C. Vandaele, N.F. Zobov, A database of water transitions from experiment and theory (IUPAC Technical Report), Pure Appl. Chem. 86 (2014) 71–83, https://doi.org/10.1515/pac-2014-5012.

[8] N. Jacquinet-Husson, R. Armante, N.A. Scott, A. Chédin, L. Crépeau, C. Boutammine, A. Bouhdaoui, C. Crevoisier, V. Capelle, C. Boonne, N. Poulet-Crovisier, A. Barbe, D. Chris Benner, V. Boudon, L.R. Brown, J. Buldyreva, A. Campargue, L.H. Coudert, V.M. Devi, M.J. Down, B.J. Drouin, A. Fayt, C. Fittschen, J.-M. Flaud, R.R. Gamache, J.J. Harrison, C. Hill, Ø. Hodnebrog, S.-M. Hu, D. Jacquemart, A. Jolly, E. Jiménez, N.N. Lavrentieva, A.-W. Liu, L. Lodi, O.M. Lyulin, S.T. Massie, S. Mikhailenko, H.S.P. Müller, O.V. Naumenko, A. Nikitin, C.J. Nielsen, J. Orphal, V.I. Perevalov, A. Perrin, E. Polovtseva, A. Predoi-Cross, M. Rotger, A.A. Ruth, S.S. Yu, K. Sung, S.A. Tashkun, J. Tennyson, V.G. Tyuterev, J. Vander Auwera, B.A. Voronin, A. Makie, The, edition of the GEISA spectroscopic database, J. Mol. Spectrosc. 327 (2016) (2015) 31–72, https://doi.org/10.1016/j.jms.2016.06.007.

[9] A.A. Kyuberis, N.F. Zobov, O.V. Naumenko, B.A. Voronin, O.L. Polyansky, L. Lodi, A. Liu, S.-M. Hu, J. Tennyson, Room temperature linelists for deuterated water, J. Quant. Spectrosc. Radiat. Transf. 203 (2017) 175–185, https://doi.org/10.1016/j.jqsrt.2017.06.026.

[10] R.A. Toth, V.D. Gupta, J.W. Brault, Line positions and strengths of HDO in the 2400–3300 cm^{-1} region, Appl. Opt. 21 (1982) 3337–3347, https://doi.org/10.1364/AO.21.003337.

[11] R.A. Toth, J.W. Brault, Line positions and strengths in the (001), (110) and (030) bands of HDO, Appl. Opt. 22 (1983) 908–926, https://doi.org/10.1364/AO.22.000908.

[12] R.A. Toth, Line positions and strengths of HDO between 6000 and 7700 cm^{-1}, J. Mol. Spectrosc. 186 (1997) 66–89, https://doi.org/10.1006/jmsp.1997.7398.

[13] R.A. Toth, HDO and D_2O low pressure, long path spectra in the 600–3100 cm^{-1} region I. HDO line positions and strengths, J. Mol. Spectrosc. 195 (1999) 73–97, https://doi.org/10.1006/jmsp.1999.7814.

[14] O.V. Naumenko, B.A. Voronin, F. Mazzotti, J. Tennyson, A. Campargue, Intracavity laser absorption spectroscopy of HDO between 12145 and 13160 cm^{-1}, J. Mol. Spectrosc. 248 (2008) 122–133, https://doi.org/10.1016/j.jms.2007.12.005.

[15] O.V. Naumenko, S. Beguier, O.M. Leshchishina, A. Campargue, ICLAS of HDO between 13020 and 14115 cm^{-1}, J. Quant. Spectrosc. Radiat. Transf. 111 (2010) 36–44, https://doi.org/10.1016/j.jqsrt.2009.06.016.

[16] L. Daumont, A. Jenouvrier, S. Mikhailenko, M. Carleer, C. Hermans, S. Fally, A.C. Vandaele, High resolution Fourier transform spectroscopy of $HD^{16}O$: Line positions, absolute intensities and selfbroadening coefficients in the 8800–11600 cm^{-1} spectral region, J. Quant. Spectrosc. Radiat. Transf. 113 (2012) 878–888, https://doi.org/10.1016/j.jqsrt.2012.02.017.

[17] V.I. Serdyukov, L.N. Sinitsa, E.R. Polovtseva, A.D. Bykov, B.A. Voronin, A.P. Scherbakov, Study of HDO absorption in the 11200–12400 cm^{-1} range using LED-based Fourier transform spectroscopy, J. Quant. Spectrosc. Radiat. Transf. 202 (2017) 187–192, https://doi.org/10.1016/j.jqsrt.2017.07.034.

[18] W.S. Benedict, N. Gailar, E.K. Plyler, Rotation-vibration spectra of deuterated water vapor, J. Chem. Phys. 24 (1956) 1139–1165, https://doi.org/10.1063/1.1742731.

[19] O.N. Ulenikov, S.-M. Hu, E.S. Bekhtereva, G.A. Onopenko, X.-H. Wang, S.-G. He, J.-J. Zhengy, Q.-S. Zhu, High-resolution Fourier transform spectrum of HDO in the Region 6140–7040 cm^{-1}, J. Mol. Spectrosc. 208 (2001) 224–235, https://doi.org/10.1006/jmsp.2001.8382.

[20] S.-M. Hu, O.N. Ulenikov, G.A. Onopenko, E.S. Bekhtereva, S.-G. He, X.-H. Wang, H. Lin, Q.-S. Zhu, High-resolution study of strongly interacting vibrational bands of HDO in the Region 7600–8100 cm-1, J. Mol. Spectrosc. 203 (2000) 228–234, https://doi.org/10.1006/jmsp.2000.8173.

[21] E. Bertseva, O. Naumenko, A. Campargue, The absorption spectrum of HDO around 1.0 μm by ICLAS-VECSEL, J. Mol. Spectrosc. 221 (2003) 38–46, https://doi.org/10.1016/S0022-2852(03)00164-4.

[22] O. Naumenko, S.-M. Hu, S.-G. He, A. Campargue, Rovibrational analysis of the absorption spectrum of HDO between 10110 and 12215 cm^{-1}, Phys. Chem. Chem. Phys. 6 (2004) 910–918, https://doi.org/10.1039/B312514A.

[23] S. Hu, H. Lin, S. He, J. Cheng, Q. Zhu, Fourier-transform intra-cavity laser absorption spectroscopy of HOD ν_{OD}=5 overtone, Phys. Chem. Chem. Phys. 1 (1999) 3727–3730, https://doi.org/10.1039/A903593A.

[24] O. Naumenko, E. Bertseva, A. Campargue, D.W. Schwenke, Experimental and ab initio studies of the HDO absorption spectrum in the 13165–13500 cm^{-1} spectral region, J. Mol. Spectrosc. 201 (2000) 297–309, https://doi.org/10.1006/jmsp.2000.8087.

[25] O. Naumenko, E. Bertseva, A. Campargue, The $4\nu_{OH}$ absorption spectrum of HDO, J. Mol. Spectrosc. 197 (1999) 122–132, https://doi.org/10.1006/jmsp.1999.7917.

[26] A.D. Bykov, V.A. Kapitanov, O.V. Naumenko, T.M. Petrova, V.I. Serdyukov, L.N. Sinitsa, The laser spectroscopy of highly excited vibrational states of $HD^{16}O$, J. Mol. Spectrosc. 153 (1992) 197–207, https://doi.org/10.1016/0022-2852(92)90468-4.

[27] O. Naumenko, A. Campargue, High-order resonance interactions in HDO: analysis of the absorption spectrum in the 14980–15350 cm^{-1} spectral region, J. Mol. Spectrosc. 199 (2000) 59–72, https://doi.org/10.1006/jmsp.1999.7982.

[28] M. Bach, S. Fally, P.F. Coheur, M. Carleer, A. Jenouvrier, A.C. Vandaele, Line parameters of HDO from high-resolution Fourier transform spectroscopy in the 11500–23000 cm^{-1} spectral region, J. Mol. Spectrosc. 232 (2005) 341–350, https://doi.org/10.1016/j.jms.2005.04.018.

[29] E. Bertseva, O. Naumenko, A. Campargue, The $5\nu_{OH}$ overtone transition of HDO, J. Mol. Spectrosc. 203 (2000) 28–36, https://doi.org/10.1006/jmsp.2000.8167.

[30] A. Jenouvrier, M.-F. Mérienne, M. Carleer, R. Colin, A.C. Vandaele, P. Bernath, O. Polyansky, J. Tennyson, The visible and near ultraviolet rotation-vibration spectrum of HOD, J. Mol. Spectrosc. 209 (2001) 165–168, https://doi.org/10.1006/jmsp.2001.8418.

[31] A. Campargue, E. Bertseva, O. Naumenko, The absorption spectrum of HDO in the 16300–16670 and 18000–18350 cm^{-1} spectral regions, J. Mol. Spectrosc. 204 (2000) 94–105, https://doi.org/10.1006/jmsp.2000.8192.

[32] R.A. Toth, Measurements of line positions and strengths of $HD^{18}O$ and $D_2^{18}O$ in the 2500–4280 cm^{-1} region, J. Mol. Struct. 742 (2005) 49–68, https://doi.org/10.1016/j.molstruc.2004.09.035.

[33] M.J. Down, J. Tennyson, J. Orphal, P. Chelin, A.A. Ruth, Analysis of an ^{18}O and D enhanced water spectrum and new assignments for $HD^{18}O$ and $D_2^{18}O$ in the near-infrared region (6000–7000 cm^{-1}) using newly calculated variational line lists, J. Mol. Spectrosc. 282 (2012) 1–8, https://doi.org/10.1016/j.jms.2012.09.006.

[34] I.A. Vasilenko, O.V. Naumenko, Absorption line lists for $HD^{18}O$ and $D_2^{18}O$ molecules based on the experimental energy levels and calculated intensities, Atmos. Ocean. Opt. 28 (2015) 496–502, https://doi.org/10.1134/S1024856015060172.

[35] V.G. Tyuterev, Y.L. Babikov, S.A. Tashkun, V.I. Perevalov, A. Nikitin, J.-P. Champion, C. Wenger, C. Pierre, G. Pierre, J.-C. Hilico, M. Loete, T.D.S. spectroscopic databank for spherical tops: DOS version, J. Quant. Spectrosc. Radiat. Transf. 52 (1994) 459–479, https://doi.org/10.1016/0022-4073(94)90174-0.

[36] M. Grossi, P. Valks, D. Loyola, B. Aberle, S. Slijkhuis, T. Wagner, S. Beirle, R. Lang, Total column water vapour measurements from GOME-2 MetOp-A and MetOp-B, Atmos. Meas. Tech. 8 (2015) 1111–1133, https://doi.org/10.5194/amt-8-1111-2015.

[37] A. Schneider, T. Borsdorff, J. Aan de Brugh, F. Aemisegger, D.G. Feist, R. Kivi, F. Hase, M. Schneider, J. Landgraf, First data set of H_2O/HDO columns from the tropospheric monitoring instrument (TROPOMI), Atmos. Meas. Tech. 13 (2020) 85–100, https://doi.org/10.5194/amt-13-85-2020.

[38] C. Borger, S. Beirle, S. Dörner, H. Sihler, T. Wagner, Total column water vapour retrieval from S-5P/TROPOMI in the visible blue spectral range, Atmos. Meas. Tech. 13 (2020) 2751–2783, https://doi.org/10.5194/amt-13-2751-2020.

[39] S.E. Fiedler, A. Hese, A.A. Ruth, Incoherent broad-band cavity-enhanced absorption spectroscopy, Chem. Phys. Lett. 371 (2003) 284–294, https://doi.org/10.1016/S0009-2614(03)00263-X.

[40] A.A. Ruth, J. Orphal, S.E. Fiedler, Cavity enhanced Fourier transform absorption spectroscopy using an incoherent broadband light source, Appl. Opt. 46 (2007) 3611–3616, https://doi.org/10.1364/AO.46.003611.

[41] J. Orphal, A.A. Ruth, High-resolution Fourier-transform cavity-enhanced absorption spectroscopy in the near-infrared using an incoherent broad-band light source, Opt. Express 16 (2008) 19232–19243, https://doi.org/10.1364/AO.46.003611.

[42] D.M. O'Leary, A.A. Ruth, S. Dixneuf, J. Orphal, R. Varma, The near infrared cavity-enhanced absorption spectrum of methyl cyanide, J. Quant. Spectrosc. Radiat. Transf. 113 (2012) 1138–1147, https://doi.org/10.1016/j.jqsrt.2012.02.022.

[43] R. Raghunandan, A. Perrin, A.A. Ruth, J. Orphal, First analysis of the $2\nu_1+3\nu_3$ band of NO_2 at 7192.159 cm^{-1}, J. Mol. Spectrosc. 297 (2014) 4–10, https://doi.org/10.1016/j.jms.2013.12.007.

[44] S. Chandran, R. Varma, Near infrared cavity enhanced absorption spectra of atmospherically relevant ether-1, 4-Dioxane, Spectrochim, Acta Part A: Mol. Biomol. Spectr. 153 (2016) 704–708, https://doi.org/10.1016/j.saa.2015.09.030.

[45] R. Raghunandan, J. Orphal, A.A. Ruth, New bands of deuterated nitrous acid (DONO) in the near-infrared using FT-IBBCEAS, Chem. Phys. Lett. X 6 (2020), https://doi.org/10.1016/j.cpletx.2020 100050.

[46] S.N. Mikhailenko, Y.L. Babikov, V.F. Golovko, Information-calculating system spectroscopy of atmospheric gases. The structure and main functions, Atmos. Oceanic Opt. 18 (2005) 685–695.

[47] N.L. Wagner, W.P. Dubé, R.A. Washenfelder, C.J. Young, I.B. Pollack, T.B. Ryerson, S.S. Brown, Diode laser-based cavity ring-down instrument for NO_3, N_2O_5, NO, NO_2 and O_3 from aircraft, Atmos. Meas. Tech. 4 (2011) 1227–1240, https://doi.org/10.5194/amt-4-1227-2011.

[48] M. Bitter, S.M. Ball, I.M. Povey, R.L. Jones, A broadband cavity ringdown spectrometer for *in-situ* measurements of atmospheric trace gases, Atmos. Chem. Phys. 5 (2005) 2547–2560, https://doi.org/10.5194/acp-5-2547-2005.

[49] R.M. Varma, D.S. Venables, A.A. Ruth, U. Heitmann, E. Schlosser, S. Dixneuf, Long optical cavities for open-path monitoring of atmospheric trace gases and aerosol extinction, Appl. Opt. 48 (2009) B159–B171, https://doi.org/10.1364/AO.48.00B159.